Parallel space-time solutions for the linear visco-acoustic and visco-elastic wave equation

Willy Dörfler, Christian Wieners, Daniel Ziegler

KARLSRUHE INSTITUTE OF TECHNOLOGY

CRC 1173

Wave
phenomena

Participating universities

Universität Stuttgart

EBERHARD KARLS
UNIVERSITÄT
TÜBINGEN

TU WIEN

Funded by

DFG

Parallel space-time solutions for the linear visco-acoustic and visco-elastic wave equation

W. Dörfler, C. Wieners and D. Ziegler

Abstract We present parallel adaptive results for a discontinuous Galerkin space-time discretization for acoustic and elastic waves with attenuation. The method is based on p-adaptive polynomial discontinuous ansatz and test spaces and a first-order formulation with full upwind fluxes. Adaptivity is controlled by dual-primal error estimation, and the full linear system is solved by a Krylov method with space-time multilevel preconditioning. The discretization and solution method is introduced in Dörfler-Findeisen-Wieners (Comput. Meth. Appl. Math. 2016) for general linear hyperbolic systems and applied to acoustic and elastic waves in Dörfler-Findeisen-Wieners-Ziegler (Radon Series Comp. Appl. Math. 2019); attenuation effects were included in Ziegler (PhD thesis 2019, Karlsruhe Institute of Technology). Here, we consider the evaluation of this method for a benchmark configuration in geophysics, where the convergence is tested with respect to seismograms. We consider the scaling on parallel machines and we show that the adaptive method based on goal-oriented error estimation is able to reduce the computational effort substantially.

1 Introduction

Classically, wave equations are considered as evolution equations where the derivative with respect to time is treated in a stronger way than the spatial differential operators. This results in an ordinary differential equation (ODE) with values in a function space with respect to the spatial variable. For example, acoustic waves in a spatial domain $\Omega \subset \mathbb{R}^d$ for a given right-hand side $\mathbf{b}$ can be considered in terms of the following ODE

$$\partial_t \mathbf{u} = A\mathbf{u} + \mathbf{b} \quad \text{in } [0, T], \quad \mathbf{u}(0) = \mathbf{0}, \qquad A = \begin{pmatrix} 0 & \text{div} \\ \nabla & 0 \end{pmatrix},$$

KIT, Fakultät für Mathematik, Englerstraße 2, 76131 Karlsruhe, e-mail: christian.wieners@kit.edu

where the solution $\mathbf{u}$ is an element of the space $C^0(0, T; \mathcal{D}(A)) \cap C^1(0, T; L_2(\Omega)^{1+d})$ with $\mathcal{D}(A) \subset H^1(\Omega) \times H_0(\mathrm{div}, \Omega)$. In order to analyze this ODE, space and time are treated separately and hence tools for partial differential equations are used in space and tools for ODEs are used in time.

Since time integration is a sequential process, we consider here for the parallelization the space-time operator

$$L(p, \mathbf{v}) = \begin{pmatrix} \partial_t p + \mathrm{div}\, \mathbf{v} \\ \partial_t \mathbf{v} + \nabla p \end{pmatrix},$$

in $Q = (0, T) \times \Omega$ as a whole treating time and space dependence simultaneously in a variational manner. Using this approach, we constructed the space-time Hilbert space $H(L, Q)$ that allows for irregular solutions, e.g., with space-time discontinuities. We select a space $V \subset H(L, Q)$ including homogeneous initial and boundary conditions such that the full space-time operator $L \colon V \longrightarrow L_2(\Omega)^{d+1}$ defines an isomorphism. As a result, for every given right-hand side $\mathbf{b} \in L_2(\Omega)^{d+1}$, the problem of finding $\mathbf{u} \in V$ such that

$$L\mathbf{u} = \mathbf{b}$$

is well-posed in our framework.

Many applications rely on accurate numerical simulations of waves through complex material structures. For instance, geophysical structures like the earth's crust below the sea bed feature complex varying material properties. A typical example is the problem of full waveform inversion (FWI), where the material distribution is reconstructed from measurements of the wave field close to the surface. This is achieved by minimizing a misfit functional. The evaluation of this functional and its gradient require wave solutions forward and backward, where the adjoint problem relies on the full information in space and time.

The forward problem for this application is considered in this work for acoustic, visco-acoustic, and visco-elastic waves. A discretization in space and time is provided by a Discontinuous Galerkin approach presented in [5]. An alternative method is the Discontinuous Petrov-Galerkin (DPG) method, which was introduced by Demkowicz et al. and provides a framework for the discretization of general linear first-order systems, see [7]. The application to acoustic waves is presented in [8, 10] and extended to heterogeneous media in [11].

2 Solving the visco-elastic wave equation in space and time

For the parallel approximation we use a space-time discretization with discontinuous ansatz functions in space and continuous ansatz functions in time together with an adaptive algorithm using dual weighted residual estimators and a multilevel preconditioner. We call this discretization the dG-cPG method, since it is discontinuous in space and continuous in time, but combined with discontinuous test functions in space and time, resulting in an Petrov–Galerkin method. A more detailed version

can be found in [6]. This discretization is applied to the acoustic and elastic wave equation in [9]. A discretization using discontinuous ansatz functions in space and time is presented in [12] and applied to the visco-acoustic and visco-elastic wave equation. We call this discretization the dG-dG method. We want to remark that the dG-cPG(q) and dG-dG($q-1$) method have the same amount of degrees of freedom, where q denotes the polynomial degree in time.

The wave equations including attenuation effects can be written in the compact operator formulation

$$L\mathbf{u} = \mathbf{b} \qquad \text{a.e. in } (0,T)$$

with $L = M\partial_t + A + D$. In the case of visco-elasticity we get

$$M(\mathbf{v}, \boldsymbol{\sigma}_0, \ldots, \boldsymbol{\sigma}_G) = \left(\rho\mathbf{v}, \mathbf{C}_0^{-1}\boldsymbol{\sigma}_0, \ldots, \mathbf{C}_G^{-1}\boldsymbol{\sigma}_G \right),$$

$$A(\mathbf{v}, \boldsymbol{\sigma}_0, \ldots, \boldsymbol{\sigma}_G) = -\left(\nabla \cdot (\boldsymbol{\sigma}_0 + \ldots + \boldsymbol{\sigma}_G), \boldsymbol{\varepsilon}(\mathbf{v}), \ldots, \boldsymbol{\varepsilon}(\mathbf{v}) \right),$$

$$D(\mathbf{v}, \boldsymbol{\sigma}_0, \ldots, \boldsymbol{\sigma}_G) = \left(\mathbf{0}, \mathbf{0}, \tau_1^{-1}\mathbf{C}_1^{-1}\boldsymbol{\sigma}_1, \ldots, \tau_G^{-1}\mathbf{C}_G^{-1}\boldsymbol{\sigma}_G \right).$$

In the special case of isotropic materials the elasticity tensors $\mathbf{C}_g = \mathbf{C}(\mu_g, \kappa_g)$ for $g = 0, \ldots, G$, with

$$\mathbf{C}(\mu, \kappa)\boldsymbol{\varepsilon} = 2\mu \, \text{dev}(\boldsymbol{\varepsilon}) + \kappa \, \text{trace}(\boldsymbol{\varepsilon})\mathbf{I}, \qquad \text{dev}(\boldsymbol{\varepsilon}) = \boldsymbol{\varepsilon} - \frac{1}{3} \, \text{trace}(\boldsymbol{\varepsilon})\mathbf{I},$$

only depend on the shear moduli μ_g and the compression moduli $\kappa_g = \lambda_g + \frac{2}{3}\mu_g$. In the limit of vanishing shear forces one obtains for the *hydrostatic pressure* $p = \frac{1}{3}\text{trace}(\boldsymbol{\sigma}) = p_0 + \cdots + p_G$ the *visco-acoustic system*

$$\rho \, \partial_t \mathbf{v} = \nabla p_0 + \cdots + \nabla p_G + \mathbf{b},$$

$$\partial_t p_0 = \kappa_0 \nabla \cdot \mathbf{v},$$

$$\partial_t p_g = \kappa_g \nabla \cdot \mathbf{v} - \frac{1}{\tau_g}p_g, \qquad g = 1, \ldots, G.$$

For the discretization, we assume that Ω is a bounded polyhedral Lipschitz domain decomposed into a finite number of open elements $K \subset \Omega$ such that $\overline{\Omega} = \bigcup_{K \in \mathcal{K}} \overline{K}$, where $\mathcal{K}$ is the set of elements in space. Let $\overline{Q} = \bigcup_{R \in \mathcal{R}} \overline{R}$ be a decomposition of the space-time cylinder into space-time cells $R = K \times I$ with $K \in \mathcal{K}$ and $I \subset [0,T]$ an interval; $\mathcal{R}$ denotes the set of space-time cells. For the fixed mesh $\mathcal{K}$ in space and a time series $0 = t_0 < t_1 < \cdots < t_N = T$, the space-time mesh is defined by

$$\mathcal{R} = \bigcup_{n=1,\ldots,N} \mathcal{R}_n, \qquad \mathcal{R}_n = \{K \times I_n : I_n := (t_{n-1}, t_n], \; K \in \mathcal{K}\}.$$

On each cell R we define the local space

$$V_{h,R} = \mathbb{P}_{p_R}(K; \mathbb{R}^J) \otimes \mathbb{P}_{q_R}(I_n; \mathbb{R}^J) \subset \mathrm{L}_2(R; \mathbb{R}^J)$$

and the global space

Algorithm 1

RCB_st(cells $\mathcal{R}$, weights $\mathcal{W}$, factor m, bisections b, sort c)

Require: $m, b \in \mathbb{N}, \ c \in \{t, x, y, z\}$
1: **if** $b == 0$ **then**
2:    send cells in $\mathcal{R}$ to process m distribute cells
3:    **return**
4: **end if**
5:   sort and bisect set of cells
6: sort $\mathcal{R}$ by coordinate c
7: split $\mathcal{R}$ into $\mathcal{R}_1$ and $\mathcal{R}_2$ such that
8:    $\sum_{R_1 \in \mathcal{R}_1} \mathcal{W}_{R_1} \approx \sum_{R_2 \in \mathcal{R}_2} \mathcal{W}_{R_2}$
9:   define coordinate for next bisection
10: **if** $c == z$ **then**
11:    $c := t$
12: **else if** $c == y$ **then**
13:    **if** dim == 3 **then**
14:       $c := z$
15:    **else**
16:       $c := t$
17:    **end if**
18: **else if** $c == x$ **then**
19:    **if** dim > 1 **then**
20:       $c := y$
21:    **else**
22:       $c := t$
23:    **end if**
24: **else**
25:    $c := x$
26: **end if**
27:   recursive call
28: RCB_st($\mathcal{R}_1, \mathcal{W}, m, b-1, c$)
29: RCB_st($\mathcal{R}_2, \mathcal{W}, m + 2^{b-1}, b-1, c$)

$$V_h = \left\{ \mathbf{v}_h \in \mathrm{L}_2((0,T); \mathrm{L}_2(\Omega; \mathbb{R}^J)) : \mathbf{v}_{h,R} = \mathbf{v}_h|_R \in V_{h,R} \right\}.$$

The polynomial degree in space and time (p_R, q_R) in each cell can be arbitrary and is chosen by an (p,q)-adaptive algorithm. The space-time cells are distributed on 2^b processes using the recursive bisection algorithm presented in Alg. 1. The algorithm combined with the appropriate choice of weights $\mathcal{W}_R$, based on the polynomial degrees (p_R, q_R), leads to a distribution, where every process has to handle the same computational effort. The space-time system is solved with a multilevel preconditioner in space and time, see [6, Chap. 6]. The parallel direct solver [2, 3, 4] is used on the coarse level.

2.1 A geophysical benchmark in heterogeneous media

The benchmark problem Marmousi II [13] for geophysical applications provides realistic structures in two space dimensions with heterogeneous media, see Fig. 1 for the density distribution in this benchmark configuration.
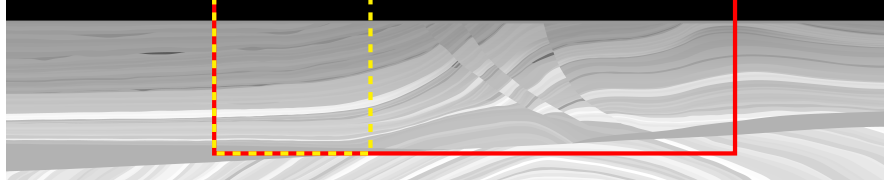

Fig. 1 Density distribution for the Marmousi II benchmark: The graphic shows the full Marmousi II benchmark with a domain size of 17 km × 3.5 km. The red subdomain 10 km × 3 km is used in the adaptive numerical experiments and the smaller yellow subdomain 3 km × 3 km for the convergence tests in space and time on uniform discretizations.

For the numerical experiments, we simulate maritime measurements in seismic exploration with a local source initiating a wave by a smooth pulse in space of width $w_s = 100$ [m] located at $\mathbf{x}_s \in \Omega$

$$\phi(\mathbf{x}) = \begin{cases} \cos^6\left(\dfrac{\pi|\mathbf{x}_s - \mathbf{x}|}{2w_s}\right) & |\mathbf{x}_s - \mathbf{x}| < w_s, \\ 0 & \text{else.} \end{cases} \tag{1}$$

and a Ricker wavelet in time

$$\psi(t) = \left(1 - 2\pi^2(t - t_s)^2 f^2\right) \exp\left(-\pi^2(t - t_s)^2 f^2\right)$$

with frequency f and time delay $t_s = 0.15$ [s]. This results in the right-hand side $\mathbf{b}(t, \mathbf{x}) = \psi(t)\,\phi(\mathbf{x})\,\mathbf{e}$ with $\mathbf{e} = (0, 1, 0, \ldots, 0) \in \mathbb{R}^{\dim+1+G}$ in the acoustic case, and $\mathbf{e} = (0, \mathbf{I}_3, 0, \ldots, 0) \in \mathbb{R}^{\dim} \times \mathbb{R}_{\text{sym}}^{\dim \times \dim} \times \cdots \times \mathbb{R}_{\text{sym}}^{\dim \times \dim}$ for elasticity.

In our tests, the solution is compared for different discretizations by the resulting pressure evaluated at the receivers positions $\mathbf{x}_{r,i} \in \Omega$, $i = 0, \ldots, N_r$. This defines a seismogram $\mathbf{s} \in L_2(0, T; \mathbb{R}^{N_r})$, i.e., $s_i(t) = p(t, \mathbf{x}_{r,i})$.

The Marmousi model prescribes a density distribution $\rho \in (1010, 2627)$ [kg/m^3] and reference values for the velocities of shear waves $v_S \in (0, 2802)$ [m/s] and compressional waves $v_P \in (1028, 4700)$ [m/s]. This defines the parameters $\mu = \rho v_S^2$ and $\kappa = \rho v_P^2 - \frac{4}{3}\mu$ for isotropic elasticity. We fix this material parameters cellwise constant on a spatial mesh with mesh size 125 [m].

We set $\kappa_0 = \frac{\kappa}{1+G\tau_P}$ and $\kappa_1 = \cdots = \kappa_G = \kappa_0 \tau_P$ with $\tau_P = 0.1$, and we set $\mu_0 = \frac{\mu}{1+G\tau_S}$ and $\mu_1 = \cdots = \mu_G = \mu_0 \tau_S$ with $\tau_S = 0.1$, Furthermore, we use the relaxation time $\tau_g = \frac{1}{2\pi f_g}$ with reference frequencies $f_1 = 0.151$ [Hz], $f_2 = 1.93$ [Hz], and $f_3 = 18.9$ [Hz], for $G = 3$ and $f_1 = 10$ [Hz] for $G = 1$.
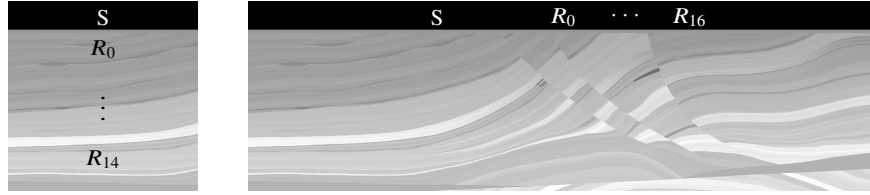
Fig. 2 Marmousi II: Sketch of location of source and receivers for the uniform computations used in the first numerical experiment on the left and for the adaptive computations used in the second experiment on the right.

2.2 Visco-acoustic equation with three damping mechanisms and uniform p-refinement

We compare the dG-dG method with the dG-cPG method on uniform discretizations with polynomial degrees p and q in space and time for the visco-acoustic model with three damping mechanisms ($G = 3$) in this numerical test. Here, we use from the full Marmousi II benchmark configuration the subdomain $\Omega = (4000, 7000) \times (-3000, 0) \subset (0, 17000) \times (-3500, 0)$ [m^2] (see the yellow dashed box in Fig. 1) and the time interval $(0, T)$ with $T = 1.5$ [s]. We use a coarse mesh in space and time with $h_0 = 1000$ [m] and $\Delta t_0 = 0.25$ [s]. The initial pulse is located at $\mathbf{x}_s = (5500, -250)$. The seismograms are measured at the receivers with the positions $\mathbf{x}_{r,i} = (5500, -750 - 125i)$ for $i = 0, \ldots, 14$.

Since we have no analytical solution for the problem, we compute the reference seismogram by extrapolation. The order of convergence on the space-time mesh of level l can be estimated from the factor

$$f_l = \frac{\|\mathbf{s}_{l-1} - \mathbf{s}_{l-2}\|_{(0,T)}}{\|\mathbf{s}_l - \mathbf{s}_{l-1}\|_{(0,T)}},$$

where $\mathbf{s}_l$ denotes the seismogram on level l combined with the L$_2$-norm. With this factor a better approximation can be constructed by extrapolation as

$$\mathbf{s}_{ex} = \frac{f_l}{f_l - 1}\mathbf{s}_l - \frac{1}{f_l - 1}\mathbf{s}_{l-1}.$$

Here we choose the fixed polynomial degrees $(p, q) = (3, 2)$ and the space-time levels $l = 3, \ldots, 5$ obtained by uniform refinement in space-time. All quantities in this test are normalized with respect to the reference value $\|\mathbf{s}_{ex}\|_{(0,T)}$.

A selection of the results of this numerical experiment are shown in Tab. 1. The results indicate, that the cPG version gives more accurate results than the dG method with one order lower in time, although both methods have the same amount of degrees of freedom. The advantage of the dG-dG method over the dG-cPG method is that the system matrix is less dense. As a result, the total time to solve the system is lower. In addition, less total system memory is required in particular with higher polynomials

dG-cPG on space-time mesh level 4					
(p,q)	e	RAM	DoF	ML	time
(2,2)	26.9%	387 GB	23 887 872	10	0:15:04
(2,3)	28.7%	753 GB	35 831 808	9	0:27:35
(3,2)	4.6%	1.0 TB	42 467 328	15	1:06:22
(3,3)	4.8%	2.2 TB	63 700 992	15	2:21:11

dG-dG on space-time mesh level 4						
(p,q)	e	$\widehat{e}$	RAM	DoF	ML	time
(2,1)	39.4%	39.1%	248 GB	23 887 872	10	0:06:48
(2,2)	28.8%	28.8%	473 GB	35 831 808	10	0:13:38
(2,3)	28.7%	28.7%	768 GB	47 775 744	10	0:22:55
(3,1)	31.1%	30.9%	636 GB	42 467 328	16	0:29:54
(3,2)	5.1%	5.1%	1.3 TB	63 700 992	15	1:02:34

Table 1 Marmousi II dG vs. cPG: comparison of the two methods on uniform discretizations. The error $e = \|\mathbf{s} - \mathbf{s}_{\mathrm{ex}}\|_{(0,T)}/\|\mathbf{s}_{\mathrm{ex}}\|_{(0,T)}$ is given in percent and in case of using the dG-dG method also the error of the seismogram obtained by evaluation of the conforming reconstruction $\widehat{e} = \|\widehat{\mathbf{s}} - \mathbf{s}_{\mathrm{ex}}\|_{(0,T)}/\|\mathbf{s}_{\mathrm{ex}}\|_{(0,T)}$. ML denotes the GMRES steps with the multilevel preconditioner. We use 10 smoothing steps if coarsened in time and 20 if coarsened in space. The time to solve the space-time system on 256 parallel cores is given in [hh:mm:ss].

in time, since the dG-dG scheme has fewer coupling between the space-time cells and thus the matrix graph is more sparse.

In Fig. 3 we illustrate the conforming reconstruction working on linear ansatz functions in time and resulting in conforming quadratic functions. The conforming reconstruction operator interpolates the ansatz functions, which are discontinuous in time, resulting in functions, which are continuous in time of one order higher as the ansatz functions. This serves the approximation order of the solution.
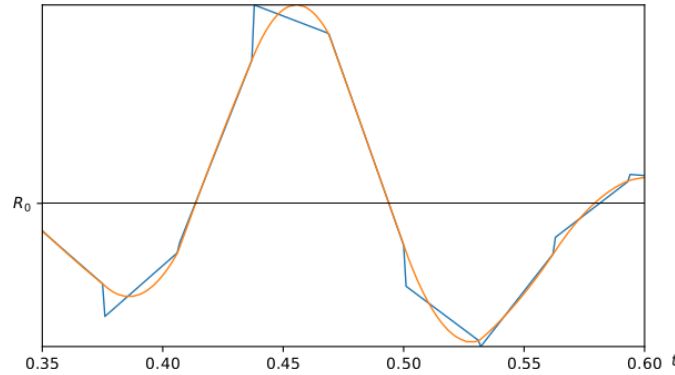

Fig. 3 Sketch of the feature using conforming reconstruction: the solution discontinuous in time obtained by the dG(p)-dG(q) method with $(p, q) = (3, 1)$ (blue) is reconstructed with Radau IIA integration points (orange).

2.3 A parallel adaptive visco-elastic computation

This numerical test demonstrates the parallel efficiency of the method. The visco-elastic system with one damping mechanism ($G = 1$) is solved using one adaptive step and the dG-cPG method.

Here we choose the domain $\Omega = (4000, 13000) \times (-3000, 0) \subset (0, 17000) \times (-3500, 0)$ [m^2] (marked red in Fig. 1) and the time interval $(0, T)$ with $T = 3$ [s]. The source is located at $\mathbf{x}_s = (7000, -250)$, and the receivers positions are $\mathbf{x}_{r,j} = (9000 + 125j, -250)$ for $j = 0, \ldots, 16$. For the adaptive simulations we use the goal functional

$$\mathcal{J}_{\text{elastic}}(\mathbf{v}, \boldsymbol{\sigma}) = \frac{1}{|\Omega_{\text{RoI}}|} \int_{\Omega_{\text{RoI}} \times \{T\}} \text{trace}\, \boldsymbol{\sigma} \, d\mathbf{x} \qquad \text{with } \boldsymbol{\sigma} = \boldsymbol{\sigma}_0 + \boldsymbol{\sigma}_1,$$

together with the region of interest $\Omega_{\text{RoI}} = (4750, 100) \times (7250, 400)$. We start with piecewise linear functions in space and time and solve the primal and dual problem. In all space-time cells where the error indicator η_R is larger than $\theta = 1 \cdot 10^{-9}$ times the largest error indicator $\eta_{\max} = \max_{R \in \mathcal{R}} \eta_R$, i.e., $\eta_R > \eta_{\text{crit}} = \theta \eta_{\max}$, the polynomial degree is increased in space and time. In contrast the polynomial degree is decreased if $\eta < 0.01 \cdot \eta_{\text{crit}}$.

The visco-elastic adaptive space-time dG-cPG simulation tracks the propagation of the wave from the source to the receivers. The first stress component (column 1) and the distribution of the polynomial degrees (p, q) (column 2) are visualized in Fig. 4. In the blue area we have $(p, q) = (0, 1)$, gray $(p, q) = (1, 1)$ and red $(p, q) = (2, 2)$.

This results into 364 Mio. degrees of freedom and the full linear space-time system is solved with 14 GMRES steps using the multilevel preconditioner (50 Gauss–Seidel smoothing steps in space and 25 Jacobi smoothing steps in time). The p-adaptive method reduces the degrees of freedom by approximately 78% compared to a uniform computation (1 968 Mio. degrees of freedom). On 4096 parallel processes the system was solved in 30 minutes and 53 seconds whereas on 8192 parallel processes the time was 15 minutes and 47 seconds. The solving time was cut nearly in half by doubling the number of processes demonstrating very good strong scaling behavior.

Conclusion

We demonstrated a nearly optimal scaling behavior for an adaptive space-time method for first-order linear hyperbolic systems. The method is realized in the parallel finite element software system M++ [1], which provides a framework for various numerical challenges such as elasticity, plasticity and electromagnetic waves. The parallel scaling for these applications which be considered in future work.
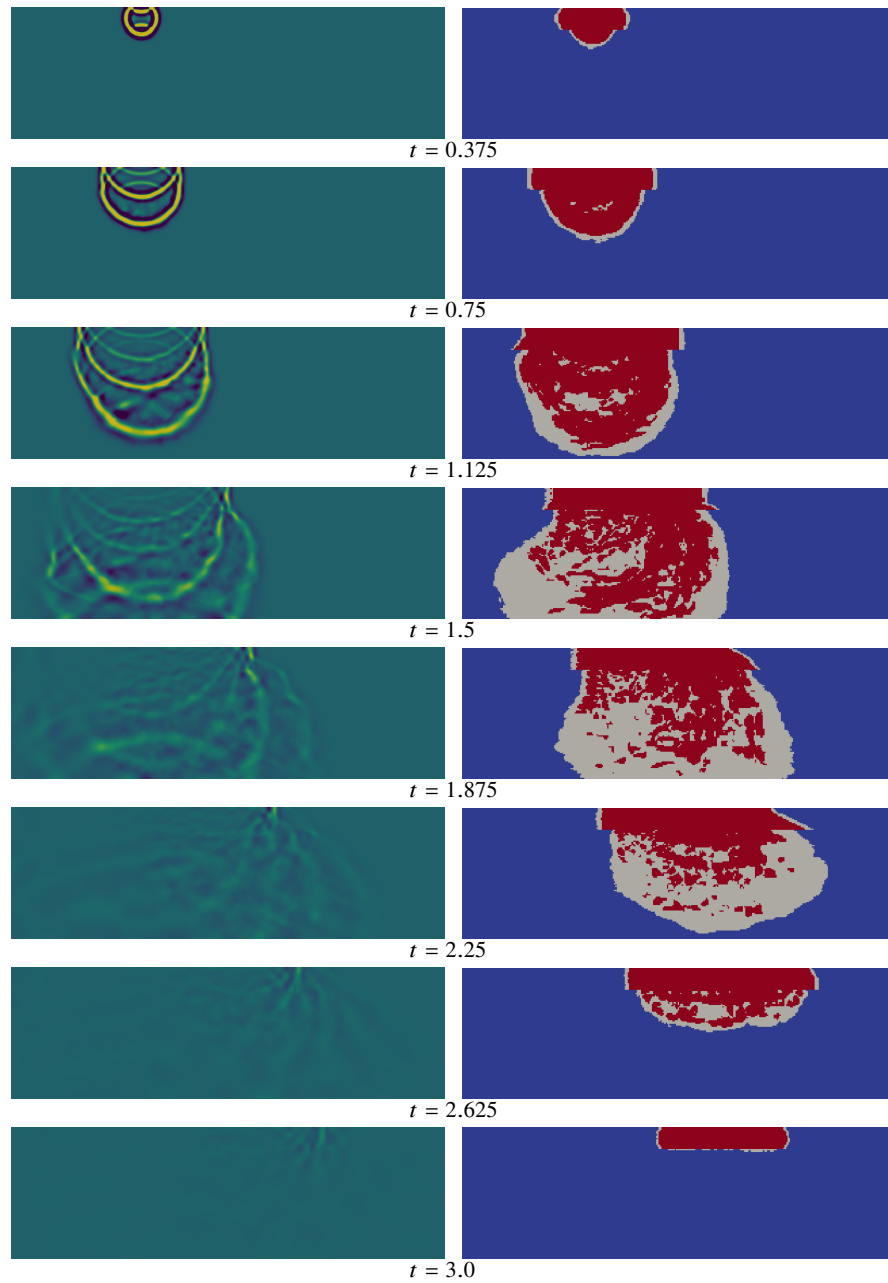
$t = 0.375$

$t = 0.75$

$t = 1.125$

$t = 1.5$

$t = 1.875$

$t = 2.25$

$t = 2.625$

$t = 3.0$

Fig. 4 Slices through the space-time solution for the visco-elastic adaptive computation at different times. On the left is the first stress component and on the right the corresponding polynomial order in space and time.

References

1. C. Wieners: A geometric data structure for parallel finite elements and the application to multigrid methods with block smoothing. In: Computing and Visualization in Science **13**, pp. 161-175, Springer (2010)
2. D. Maurer and C. Wieners: Parallel Multigrid Methods and Coarse Grid LDL^T Solver for Maxwell's Eigenvalue Problem. In: C. Bischof, H. Hegering, W. Nagel and G. Wittum (eds.) Competence in High Performance Computing 2010, pp. 205-213, Springer (2010)
3. D. Maurer and C. Wieners: A parallel block LU decomposition method for distributed finite element matrices. In: Parallel Computing **37**, pp. 742-758 (2011)
4. D. Maurer and C. Wieners: A Highly Scalable Multigrid Method with Parallel Direct Coarse Grid Solver for Maxwell's Equations. In: W. Nagel, D. Kröner and M. Resch (eds.) High Performance Computing in Science and Engineering '13, Transactions of the High Performance Computing Center, Stuttgart (HLRS) 2013, pp. 671-677, Springer (2013)
5. W. Dörfler, S. Findeisen and C. Wieners: Space-time discontinuous Galerkin discretizations for linear first-order hyperbolic evolution systems. In: Comput. Methods Appl. Math. **16**, pp. 409-428 (2016)
6. S. Findeisen: A Parallel and Adaptive Space-Time Method for Maxwell's Equations. PhD thesis, Karlsruhe Institute of Technology (KIT), Karlsruhe (2016)
7. C. Wieners: The Skeleton Reduction for Finite Element Substructuring Methods. In: B. Karasözen, M. Manguoğlu, M. Tezer-Sezgin, S. Göktepe and Ö. Uğur (eds.) Numerical Mathematics and Advanced Applications ENUMATH 2015, pp. 133-141, Springer International Publishing (2016)
8. J. Ernesti: Space-Time Methods for Acoustic Waves with Applications to Full Waveform Inversion. PhD thesis, Karlsruhe Institute of Technology (KIT), Karlsruhe (2018)
9. W. Dörfler, S. Findeisen, C. Wieners and D. Ziegler: Parallel adaptive discontinuous Galerkin discretizations in space and time for linear elastic and acoustic waves. In: U. Langer and O. Steinbach (eds.) Space-Time Methods. Applications to Partial Differential Equations, pp. 61-88. Walter de Gruyter, Radon Series on Computational and Applied Mathematics **25** (2019)
10. J. Ernesti and C. Wieners: A space-time discontinuous Petrov–Galerkin method for acoustic waves. In: U. Langer and O. Steinbach (eds.) Space-Time Methods. Applications to Partial Differential Equations, pp. 89-116. Walter de Gruyter, Radon Series on Computational and Applied Mathematics **25** (2019)
11. J. Ernesti and C. Wieners: Space-time discontinuous Petrov–Galerkin methods for linear wave equations in heterogeneous media. Karlsruhe Institute of Technology (KIT), CRC 1173 (2019)
12. D. Ziegler: A Parallel and Adaptive Space-Time Discontinuous Galerkin Method for Visco-Elastic and Visco-Acoustic Waves. PhD thesis, Karlsruhe Institute of Technology (KIT), Karlsruhe (2019)
13. G. Martin, R. Wiley and K. Marfurt: Marmousi2: An elastic upgrade for Marmousi. In: The Leading Edge **25**, pp. 156-166 (2006)